

---

# $\pi$ VAE: Encoding stochastic process priors with variational autoencoders

---

**Swapnil Mishra\***

School of Public Health  
Imperial College London  
s.mishra@imperial.ac.uk

**Seth Flaxman\***

Department of Mathematics  
Imperial College London  
s.flaxman@imperial.ac.uk

**Samir Bhatt\***

School of Public Health  
Imperial College London  
s.bhatt@imperial.ac.uk

## Abstract

Stochastic processes provide a mathematically elegant way to model complex data. In theory, they provide flexible priors over function classes that can encode a wide range of interesting assumptions. However, in practice efficient inference by optimisation or marginalisation is difficult, a problem further exacerbated with big data and high dimensional input spaces. We propose a novel variational autoencoder (VAE) called the prior encoding variational autoencoder ( $\pi$ VAE). The  $\pi$ VAE is finitely exchangeable and Kolmogorov consistent, and thus is a continuous stochastic process. We use  $\pi$ VAE to learn low dimensional embeddings of function classes. We show that our framework can accurately learn expressive function classes such as Gaussian processes, but also properties of functions to enable statistical inference (such as the integral of a log Gaussian process). For popular tasks, such as spatial interpolation,  $\pi$ VAE achieves state-of-the-art performance both in terms of accuracy and computational efficiency. Perhaps most usefully, we demonstrate that the low dimensional independently distributed latent space representation learnt provides an elegant and scalable means of performing Bayesian inference for stochastic processes within probabilistic programming languages such as Stan.

## 1 Introduction

A central task in machine learning is to specify a function or set of functions that best generalises to new data. Stochastic processes [1] provide a mathematically elegant way to define a class of functions, where each element from a stochastic process is a (usually infinite) collection of random variables. Popular examples of stochastic processes in machine learning are Gaussian processes [2], Dirichlet processes [3], log Gaussian-Cox processes [4], Hawkes processes [5], Mondrian processes [6] and Gauss-Markov processes [7]. Many of these processes are intimately connected with popular techniques in deep learning, for example, both the infinite width limit of a single layer neural network and the evolution of a deep neural network by gradient descent are Gaussian processes [8, 9]. However, while stochastic processes have many favourable properties, they are often cumbersome to work with in practice. For example, inference and prediction using a Gaussian process requires matrix inversions that scale cubically with data size, log Gaussian Cox processes require the evaluation of an intractable integral and Markov processes are often highly correlated. Bayesian inference can be even more challenging due to complex high dimensional posterior topologies. Gold standard

---

\*equal contribution

evaluation of posterior expectations is done by Markov Chain Monte Carlo (MCMC) sampling, but high auto-correlation, narrow typical sets [10] and poor scalability have prevented use in big data/model settings. A plethora of approximation algorithms exists [11–15], but few have asymptotic guarantees and, more troubling, even fewer actually yield accurate posterior estimates [16–19]. In this paper, rather than relying on approximate Bayesian inference to solve complex models, we extend variational autoencoders (VAE) [20, 21] to develop portable models that can work with state-of-the-art Bayesian MCMC software such as Stan [22]. Inference on the resulting models is tractable and yields accurate posterior expectations and uncertainty.

An autoencoder [23] is a model comprised of two component networks  $\eta$ : The encoder  $\eta_e : \mathcal{X} \rightarrow \mathcal{Z}$  and a decoder  $\eta_d : \mathcal{Z} \rightarrow \mathcal{X}$  where the latent space  $\mathcal{Z}$  is typically of much lower dimension than  $\mathcal{X}$ . The autoencoder is then learnt through the minimisation of a loss function  $\mathcal{L}$ . A VAE extends the autoencoder into a generative model [20]. In a VAE, the latent variables  $\mathcal{Z}$  are independent normally distributed random variables with parameters from the encoder, and a variational approximation of the posterior is estimated. In a variety of applications, VAEs fit well to the trained data and enable the generation of new data by sampling from the latent space; a mechanism that makes it a popular tool for probabilistic modelling [24]. In this paper we propose a novel use of VAEs: we learn low dimensional representations of samples from a given function class (e.g. sample paths from a Gaussian process prior). We then use the resulting low dimensional representation and the decoder to perform Bayesian inference.

One key benefit of this approach is that we decouple the prior from inference to encode arbitrarily complex prior function classes, without needing to calculate any data likelihoods. A second key benefit is that when inference is performed, our sampler operates in a low dimensional, uncorrelated latent space which greatly aids efficiency and computation. One limitation of this approach is that we are restricted to encoding finite-dimensional priors, because VAEs are not stochastic processes. To overcome this limitation, we introduce a new VAE called the prior encoding VAE ( $\pi$ VAE) that satisfies exchangeability and Kolmogorov consistency and is thus a valid stochastic process by the Kolmogorov extension theorem.

The most relevant approach to ours is the neural process [25] which, similar to Gaussian processes, tries to learn a distribution over functions. The neural process is a stochastic process that fits to data while simultaneously learning the function class (estimating the prior and posterior simultaneously). In functional form, it is similar to a VAE except, in neural processes, the KL divergence penalty term is the divergence from training and testing latent variables (as opposed to a standard normal in a VAE) and an aggregation step is included to allow for exchangeability and consistency. A key theoretical limitation of neural processes is that their accuracy is hindered by variation inference, which provides no guarantees that the estimated posterior distribution is correct. In addition neural processes often learn functions that substantially underfit and therefore tend to predict both point estimates and uncertainty inaccurately [26]. In contrast to the neural process, we employ a two step approach: first, we encode the prior using a VAE; second we combine the learnt decoder network with a likelihood in a fully Bayesian modeling framework, and use MCMC to fit our model. We believe our framework’s novel decoupling of the prior and the inference is critically important for many complex scenarios.

Once a  $\pi$ VAE is trained and defined, the complexity of the decoder scales linearly in the size of the largest hidden layer. Additionally, because the latent variables are penalised via the KL term from deviating from standard Gaussians, the latent space is approximately uncorrelated, leading to high effective sample sizes in MCMC sampling. The main contributions of this paper are:

- We apply the generative framework of VAEs to perform full Bayesian inference. We first encode priors in training and then, given new data, perform inference on the latent representation while keeping the trained decoder fixed.
- We propose a new generative model,  $\pi$ VAE, that generalizes VAEs to be able to learn priors over both functions and properties of functions. We show that  $\pi$ VAE satisfies the Kolmogorov extension theorem and is therefore a stochastic process.
- Finally, we show the performance of  $\pi$ VAE on a range of simulated and real data, and show that  $\pi$ VAE achieves state-of-the-art performance in a spatial interpolation task.

The rest of this paper is structured as follows. Section 2 details the proposed framework and the generative model along with toy fitting examples. The experiments on large real world datasets are outlined in Section 3. We discuss our findings and conclude in Section 4.

## 2 Methods

### 2.1 Variational Autoencoders (VAEs)

A standard VAE has three components, an encoder network ( $e(\cdot)$ ) with parameters  $\eta_e$ , random variables  $\mathcal{Z}$ , and a decoder network ( $d(\cdot)$ ) with parameters  $\eta_d$ . In many settings, given an input,  $x \in \mathbb{R}$  (e.g. a flattened image or discrete time series),  $e(\eta_e, x)$  and  $d(\eta_d, \mathcal{Z})$  are simply multilayer perceptrons, but can be more complicated and include convolution or recurrent layers. The output of the encoder network are parameters which can be used to create random variables  $\mathcal{Z}$ : a latent representation of  $x$  in a lower-dimensional (Gaussian) probabilistic space. The decoder network takes random variables and tries to reconstruct the input by producing  $\hat{x}$ . Putting both the encoder and decoder together results in the following model

$$\begin{aligned} [z_\mu, z_{sd}]^\top &= e(\eta_e, x) \\ \mathcal{Z} &\sim \mathcal{N}(z_\mu, z_{sd}^2 \mathbb{I}) \\ \hat{x} &= d(\eta_d, \mathcal{Z}). \end{aligned} \quad (1)$$

End to end, Eq. 1 can be compactly expressed as  $\hat{x} = d(\eta_d, e(\eta_e, x))$ . To train a VAE, a variational approximation is used to estimate the posterior distribution  $p(\mathcal{Z}|x, \eta_d, \eta_e) \propto p(x|\mathcal{Z}, \eta_d, \eta_e)p(\mathcal{Z})$ . The variational approximation greatly simplifies inference by turning a marginalisation problem into an optimisation problem. The optimal parameters for the encoder and decoder are found by maximising the evidence lower bound:

$$\arg \max_{\eta_e, \eta_d} p(x|\mathcal{Z}, \eta_d, \eta_e) - \text{KL}(\mathcal{N}(z_\mu, z_{sd}^2 \mathbb{I}) \parallel \mathcal{N}(0, \mathbb{I})) \quad (2)$$

The first term in Eq. 2 is the likelihood quantifying how well  $\hat{x}$  matches  $x$ . The second term is a Kullback-Leibler divergence penalty to ensure that  $\mathcal{Z}$  is as similar as possible to the prior distribution, a standard normal. Once fully trained on a set of samples, we fix  $\eta_d$ , and use the decoder as a generative model. To simplify subsequent notation we refer to a fully trained decoder as  $d$  and when evaluated as  $d(\cdot)$ . Generating a new sample vector  $v$  is simple: First draw a random variable  $\mathcal{Z} \sim \mathcal{N}(0, \mathbb{I})$  and then perform a deterministic transformation via the decoder  $v = d(\mathcal{Z})$ .

VAEs have been typically used in the literature to create or learn a generative model of observed data [20]. However, here we introduce a novel application of VAEs to use them for Bayesian inference on new data after learning a prior over random vectors. In this role we first train a VAE on random vectors from an easy to simulate space such as a reproducing kernel Hilbert space (samples from a Gaussian process). Training a VAE embeds these vectors in a lower dimensional probabilistic space. Once fully trained, sampling random variables from this lower dimensional space and transforming via the decoder would then be able to generate new random vectors. This decoder end of the VAE can therefore be used to perform inference on a new “data” vector,  $y$ , where the parameters of the decoder are fixed, and the latent space is trainable. In this inferential scheme the unnormalised posterior distribution of  $\mathcal{Z}$  is:

$$p(\mathcal{Z}|y, d) \propto p(y|d, \mathcal{Z})p(\mathcal{Z}). \quad (3)$$

In the standard VAE approach introduced above, we have:

$$p(z_\mu, z_{sd}|y, d) \propto p(y|d, z_\mu, z_{sd})\mathcal{N}(z_\mu, z_{sd}^2 \mathbb{I}).$$

Note that the observation model  $p(y|d, \mathcal{Z})$  in Eq. (3) could be generalised to include an additional parameter to account for the observation error. It is useful to contrast the inference task from Eq. (3) to a Bayesian neural network (BNN) [9] or Gaussian process in primal form [27]. In a BNN, with weights and biases  $\omega$ , with prior hyperparameters  $\lambda$ , the unnormalised posterior would be

$$p(\omega, \lambda|s, y) \propto p(y|s, \omega, \lambda)p(\omega|\lambda)p(\lambda). \quad (4)$$

The key difference between Eq. (4) and Eq. (3) is the term  $p(\omega|\lambda)$ .  $\omega$  is typically huge, sometimes in the millions, and is conditional on  $\lambda$ , where as in Eq. (3) the latent dimension of  $\mathcal{Z}$  is typically small ( $< 50$ ), uncorrelated and unconditioned. Given the sizes of  $\omega$  full batch MCMC training is difficult and approximation algorithms tend to poorly capture the complex posterior [19, 16]. Additionally,  $\omega$  tends to be highly correlated, making efficient MCMC nearly impossible. Finally, as the dimension and depth increases the posterior distribution suffers from complex multimodality,

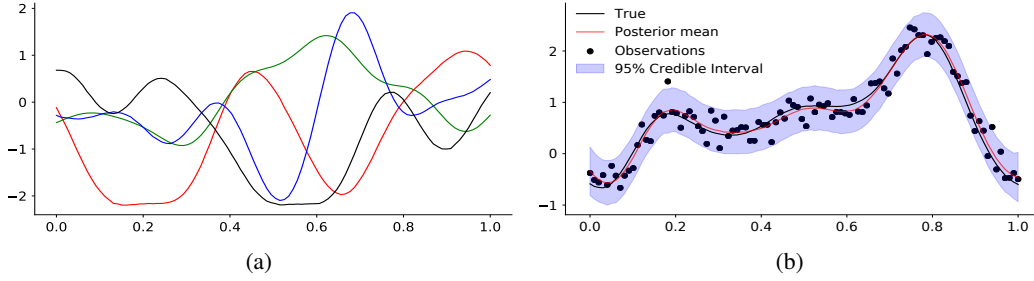


Figure 1: Learning functions with VAE: (a) Prior samples from a VAE trained on Gaussian process samples (b) we fit our VAE model to data drawn from a GP (blue) plus noise (black points). The posterior mean of our model is in red with the 95% epistemic credible intervals shown in purple.

and concentration to a narrow typical set [10]. By contrast, off-the-shelf MCMC methods like Stan [22] are very effective for equation (3), since they simply need to sample from a multidimensional Gaussian distribution, while the complexity is accounted for by the deterministic decoder.

An example of using VAEs to perform inference is shown in Fig. 1 where we train a VAE ( $Z = 10$ ) on samples drawn from a zero mean Gaussian process with RBF kernel ( $K(\delta) = e^{-\delta^2/8^2}$ ). In Fig. 1 we closely recover the true function and correctly estimate the data noise parameter. Our MCMC samples showed virtually no autocorrelation, and all diagnostic checks were excellent (see Appendix [28]). Solving the equivalent problem using a Gaussian process prior would not only be considerably more expensive ( $\mathcal{O}(n^3)$ ) but correlations in the parameter space would complicate MCMC sampling and necessitate very long chains to achieve even modest effective sample sizes.

While this simple example might seem useful, inference and prediction using a VAEs will not be possible if new input locations are required, or if the input locations are permuted. These limitations occur because a VAE is not a valid stochastic process in the sense of the Kolmogorov extension theorem. To overcome these problems we introduce a new extension to VAE called  $\pi$ VAE that is capable of learning a stochastic process class of functions.

## 2.2 The stochastic process prior encoding Variational Autoencoder - $\pi$ VAE

To create a VAE with the ability to perform inference on a wide range of problems we have to ensure exchangeability and Kolmogorov consistency. Previous attempts to do this have relied on introducing an aggregation (typically an average) to create an order invariant global distribution [25]. However, as noted by [26], this can lead to underfitting. For  $\pi$ VAE we learn a feature mapping  $\Phi$  over the input space. This ensures that  $\pi$ VAE is a valid stochastic process (see theorem 1 and theorem 2). To convert a VAE into a stochastic process, instead of directly learning mappings of function values at a fixed set of locations, we first learn a feature map and then a linear mapping from this feature map to the observed values of the function. The autoencoder learns a latent probabilistic representation over the linear mappings.

We use  $(s, x)$  to denote any arbitrary pair of (input,output) locations. Let us assume, without loss of generality, we have  $N$  function draws where each function is evaluated at  $K$  different locations<sup>2</sup>. In the encoder we transform each observed location for a function  $s_i^k$ , where  $i \in N$  and  $k \in K$ , to a fixed feature space through a transformation function  $\Phi(s_i^k)$  that is shared for all  $s \in S$  locations across all  $N$  functions.  $\Phi(s)$  could be an explicit feature representation for an RKHS (e.g. an RBF network or a random Fourier feature basis [27]), a neural network of arbitrary construction or, as we use in the examples in this paper, a combination of both. Following this transformation, a linear basis  $\beta$  is used to predict function evaluations at an arbitrary set of locations  $s$ . The intuition behind these two transformations is to learn the association between locations and observations. In contrast to a standard VAE encoder that takes as input function evaluations,  $[z_\mu, z_{sd}]^\top = e(\eta_e, x_i)$  and encodes these to a latent space,  $\pi$ VAE encoder first transforms the locations to a higher dimensional feature space via  $\Phi$ , and then connects this feature space to outputs,  $x$ , through a linear mapping,  $\beta$ . The  $\pi$ VAE decoder takes outputs from the encoder, and attempts to recreate  $\beta$  from a lower dimensional

<sup>2</sup>The number of evaluation across each function can change in our model, all equations would still hold if  $K$  is conditioned on  $n \in N$  to be  $K_n$ .

probabilistic embedding. This recreation,  $\hat{\beta}$ , is then used as a linear mapping with the *same*  $\Phi$  to get a reconstruction of the outputs  $\hat{x}$ . It is crucial to note that a single  $\beta$  vector is *not* learnt. Instead, for each function in  $i \in N$  a  $\beta_i$  is learnt. End-to-end  $\pi$ VAE is:

$$\begin{aligned}\hat{x}_{e,i}^k &= \beta_i^\top \Phi(s_i^k) \\ [z_\mu, z_{sd}]^\top &= e(\eta_e, \beta_i) \\ \mathcal{Z} &\sim \mathcal{N}(z_\mu, z_{sd}^2 \mathbb{I}) \\ \hat{\beta}_i &= d(\eta_d, \mathcal{Z}) \\ \hat{x}_{d,i}^k &= \hat{\beta}_i^\top \Phi(s_i^k).\end{aligned}\tag{5}$$

It can be seen from Eq. 5 that the central task is not, as in the VAE, to recreate the input (note  $\hat{x}$  in both ends of  $\pi$ VAE) but to reconstruct the linear parameters  $\beta$  that can map a shared  $\Phi$  onto the inputs. End to end learning is performed in  $\pi$ VAE to estimate parameters for  $\eta_e, \eta_d, \Phi$  and  $\beta$ . The evidence lower bound to be maximised is similar to that for the VAE, except the likelihood term now has an additional term for the reconstructing via feature transformation and linear mapping.

$$\arg \max_{\eta_e, \eta_d, \Phi, \beta_i} p(x_i^k | \beta_i, s_i^k, \phi, \eta_e) + p(x_i^k | \mathcal{Z}, s_i^k, \phi, \eta_d) - \text{KL}(\mathcal{N}(z_\mu, z_{sd}^2 \mathbb{I}) \| \mathcal{N}(0, \mathbb{I}))\tag{6}$$

When assuming a Gaussian likelihood, Eq. 6 can be simplified to the following loss function:

$$\arg \min_{\eta_e, \eta_d, \Phi, \beta} (x_i^k - \beta_i^\top \Phi(s_i^k))^2 + (x_i^k - \hat{\beta}_i^\top \Phi(s_i^k))^2 + \text{KL}(\mathcal{N}(z_\mu, z_{sd}^2 \mathbb{I}) \| \mathcal{N}(0, \mathbb{I}))\tag{7}$$

In Eq. 7, the first term ensures a minimum square error of the linear mapping ( $\beta$ ) of  $\Phi$  and the input. The second term ensures a minimum square error of the reconstructed ( $\hat{\beta}$ ) linear mapping of  $\Phi$  and the input. The third term is a KL loss to ensure the latent dimension is as close to  $\mathcal{N}(0, \mathbb{I})$  as possible. Once again it is important to note the indices  $i$ . A different  $\beta_i$  is learnt for every function draw  $(x_i, s_i)$  but the same  $\Phi$  is used. This means we need to learn  $\eta_e, \eta_d, \Phi$  but also  $N$   $\beta$ s, one for each sample function. While this may seem like a huge computational task,  $K$  is typically quite small ( $< 200$ ) and so learning can be relatively quick (dominated by matrix multiplication of hidden layers).

The  $\pi$ VAE can be used as a generative model. Generating a function  $f$  is done by first, selecting input locations,  $s$ , and then drawing  $z \sim \mathcal{N}(0, \mathbb{I})$ . This sample  $z$  is then transformed into a sample through a deterministic transformation via the decoder and  $\Phi$ ,  $f(\cdot) := d(z)^\top \Phi(\cdot)$ . The  $\pi$ VAE can be used for inference on new data pairs  $(s_j, y_j)$ , where the unnormalised posterior distribution is

$$\begin{aligned}p(\mathcal{Z} | d, y_j, s_j, \Phi) &\propto p(y_j | d, s_j, \mathcal{Z}, \Phi) p(\mathcal{Z}) \\ p(z_\mu, z_{sd} | d, y_j, s_j, \Phi) &\propto p(y_j | d, s_j, z_\mu, z_{sd}, \Phi) \mathcal{N}(z_\mu, z_{sd}^2 \mathbb{I})\end{aligned}\tag{8}$$

We note,  $(s_j, y_j)$  is a *set* of observed data, i.e., it is a collection of (input, output) locations from a new unknown function that is to be inferred. Further, the distinguishing difference between Eq. (3) and Eq. (8) is conditioning on input locations and  $\Phi$ . It is  $\Phi$  that ensures  $\pi$ VAE is a valid stochastic process. We formally prove this below:

**Theorem 1 (Exchangeability)** *Consider a permutation function  $\pi$ , locations  $s_1, \dots, s_n$ , fixed and bounded functions  $\Phi$  and  $d$ , and a multivariate Gaussian random variable  $\mathcal{Z}$ . Together, these define the random function  $f(\cdot) = d(\mathcal{Z})^\top \Phi(\cdot)$ . To lighten notation below we define  $f(s_i) := f_i$ . We claim:  $p(f_1, \dots, f_n) = p(f_{\pi(1)}, \dots, f_{\pi(n)})$ .*

$$\begin{aligned}\text{Proof. } p(f_1, \dots, f_n) &= \int_{\mathcal{Z}} p(f_1, \dots, f_n | \mathcal{Z}) p(\mathcal{Z}) d\mathcal{Z} = \int_{\mathcal{Z}} \prod_{i=1}^n p(d(\mathcal{Z})^\top \Phi(s_i) | \mathcal{Z}) p(\mathcal{Z}) d\mathcal{Z} \\ &= \int_{\mathcal{Z}} p(f_{\pi(1)}, \dots, f_{\pi(n)} | \mathcal{Z}) p(\mathcal{Z}) d\mathcal{Z} = p(f_{\pi(1)}, \dots, f_{\pi(n)})\end{aligned}$$

Where the second equality follows by the definition of  $f$ .  $\square$

**Theorem 2 (Consistency)** *Under the same conditions as Theorem 1, and given an extra location  $s_{n+1}$  we claim:  $p(f_1, \dots, f_n) = \int_{f_{n+1}} p(f_1, \dots, f_{n+1}) df_{n+1}$ .*

$$\begin{aligned}
\text{Proof. } \int_{f_{n+1}} p(f_1, \dots, f_{n+1}) df_{n+1} &= \int_{f_{n+1}} \int_{\mathcal{Z}} p(f_1, \dots, f_{n+1} | \mathcal{Z}) p(\mathcal{Z}) d\mathcal{Z} df_{n+1} \\
&= \int_{f_{n+1}} \int_{\mathcal{Z}} \prod_{i=1}^n p(d(\mathcal{Z})^\top \Phi(s_i) | \mathcal{Z}) p(d(\mathcal{Z})^\top \Phi(s_{i+1}) | \mathcal{Z}) p(\mathcal{Z}) d\mathcal{Z} df_{n+1} \\
&= \int_{\mathcal{Z}} \prod_{i=1}^n p(d(\mathcal{Z})^\top \Phi(s_i) | \mathcal{Z}) p(\mathcal{Z}) \int_{f_{n+1}} p(d(\mathcal{Z})^\top \Phi(s_{i+1}) | \mathcal{Z}) df_{n+1} d\mathcal{Z} \\
&= \int_{\mathcal{Z}} \prod_{i=1}^n p(d(\mathcal{Z})^\top \Phi(s_i) | \mathcal{Z}) p(\mathcal{Z}) d\mathcal{Z} = p(f_1, \dots, f_n) \quad \square
\end{aligned}$$

We first demonstrate the utility of our proposed  $\pi$ VAE model by fitting the simulated 1-D regression problem introduced in [29]. The training points for the dataset are created by uniform sampling of 20 inputs,  $x$ , between  $(-4, 4)$ . The corresponding output is set as  $y \sim \mathcal{N}(x^3, 9)$ . We fit two different variants of  $\pi$ VAE, representing two different prior classes of functions. The first prior produces cubic monotonic functions and the second prior is a GP with an RBF kernel and a two layer neural network. We generated  $10^4$  different function draws from both priors to train the respective  $\pi$ VAE. One important consideration in  $\pi$ VAE is to choose a sufficiently expressive  $\Phi$ , we used a RBF layer with trainable centres coupled with two layer neural network with 20 hidden units each. We compare our results against 20,000 Hamiltonian Monte Carlo (HMC) samples [30] implemented using Stan [22]. Details for the implementation for all the models can be found in the Appendix [28].

Fig. 2(a) presents results for  $\pi$ VAE with a cubic prior, Fig. 2(b) with the GP+NN prior, and Fig. 2(c) for a standard RBF + HMC. Both, the mean estimates and the uncertainty from  $\pi$ VAE variants, are closer, and more constrained than the ones using HMC. Importantly,  $\pi$ VAE with cubic prior not only produces better point estimates but is able to capture better uncertainty bounds. This demonstrates that  $\pi$ VAE can be used to incorporate domain knowledge about the functions being modelled.

In many scenarios, learning just the mapping of inputs to outputs is not sufficient as other functional properties are required to perform useful (interesting) analysis. For example, using point processes requires knowing the underlying intensity function, however, to perform inference we need to calculate the integral of that intensity function too. Calculating this integral, even in known analytical form, is very expensive. Hence, in order to circumvent the issue, we use  $\pi$ VAE to learn both function values and its integral for the observed events. Figure 3 shows  $\pi$ VAE prediction for both the intensity and integral of a simulated 1-D Log Gaussian Cox Process (LGCP).

In order to train  $\pi$ VAE to learn from the function space of 1-D LGCP functions, we first create a training set by drawing 10,000 different samples of the intensity function using an RBF kernel for 1-D LGCP. For each of the drawn intensity function, we choose an appropriate time horizon to sample 80 observed events (locations) from the intensity function. The  $\pi$ VAE is trained on the sampled 80 locations with their corresponding intensity and the integral. The  $\pi$ VAE therefore outputs both the instantaneous intensity and the integral of the intensity. The implementation details can be seen in the Appendix [28]. For testing, we first draw a new intensity function (1-D LGCP) using the same mechanism used in training and sample 100 events (locations). As seen in Fig. 3 our estimated intensity is very close to true intensity and even the estimated integral is close to the true integral. This example shows that the  $\pi$ VAE approach can be used to learn not only function evaluations but properties of functions.

### 3 Results

#### 3.1 Examples

Here we show applications of  $\pi$ VAE on three real world datasets. In our first example we use  $\pi$ VAE to predict the deviation in land surface temperature in East Africa [31]. We have the deviation in land surface temperatures for  $\sim 89,000$  locations across East Africa. Our training data consisted of 6,000 uniformly sampled locations. Temperature was predicted using only the spatial locations as inputs. Fig. 4 shows the results of the ground truth (a), our  $\pi$ VAE (b), a full rank Gaussian process with Matérn kernel [32], and low rank Gauss Markov random field (a widely used approach in the field of geostatistics) with 1,046 ( $\frac{1}{6}$ th of the training size) basis functions [7, 33]. We train our  $\pi$ VAE model on  $10^7$  functions draws from 2-D GP with small lengthscales between  $10^{-5}$  to 2.  $\Phi$  was set to be a

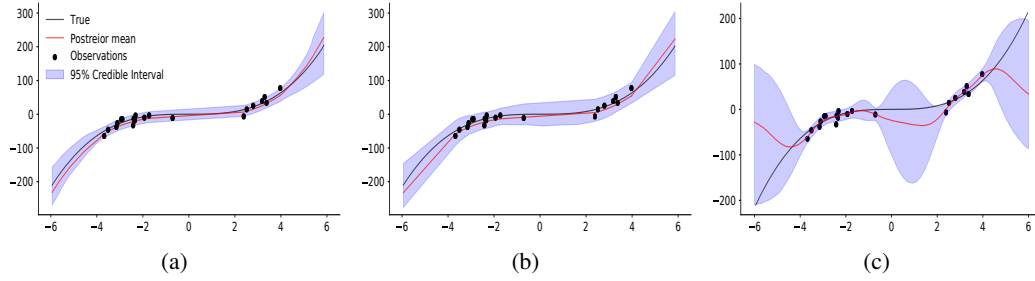


Figure 2: The true underlying function is  $y \sim \mathcal{N}(x^3, 9)$ . (a)  $\pi$ VAE trained on a class of cubic functions, (b)  $\pi$ VAE trained on samples from a Gaussian process with RBF kernel and (c) is a Gaussian process with RBF kernel fit with HMC

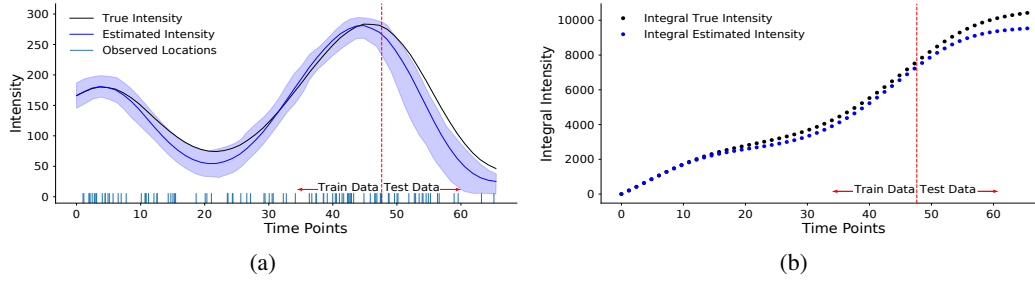


Figure 3: Inferring the intensity of a log Gaussian Cox Process. (a) compares the posterior distribution of the intensity estimated by  $\pi$ VAE to the true intensity function on train and test data. (b) compares the posterior mean of the cumulative integral over time estimated by  $\pi$ VAE to the true cumulative integral on train and test data.

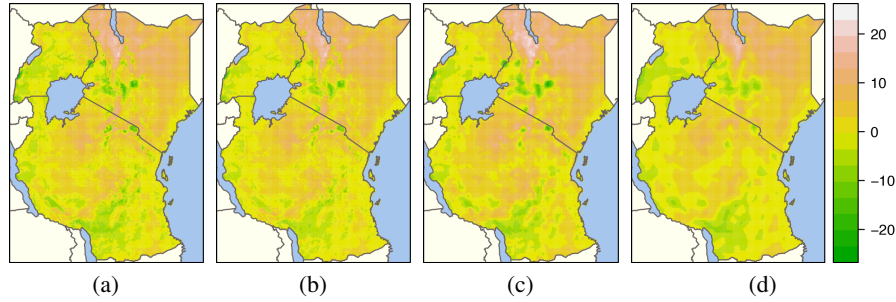


Figure 4: Deviation in land surface temperature for East Africa trained on 6000 random uniformly chosen locations [31]. Plot (a) is the data, (b) is our  $\pi$ VAE approach (testing MSE: 0.38), (c) is a full rank GP with Matérn  $\frac{3}{2}$  kernel (testing MSE: 2.47) and (d) is a low rank SPDE approximation with 1953 basis functions [7] and a Matérn  $\frac{3}{2}$  kernel (testing MSE: 2.91). The  $\pi$ VAE not only has a substantially lower test error but captures fine scale features much better than a Gaussian process.

Matérn layer with 1,000 centres followed by a two layer neural network of 100 hidden units in each layer. The  $\pi$ VAE latent dimension was set to 20. As seen in Fig. 4,  $\pi$ VAE is able to capture small scale features and produces a far better reconstruction than the both full and low rank GP and despite having a much smaller latent dimension of 20 vs 6,000 (full) vs 1,046 (low). The testing error is substantially better than the full rank GP which begs the question, why does  $\pi$ VAE perform so much better than a GP, despite being trained on samples from a GP? One possible reason is that the extra hidden layers in  $\Phi$  create a much richer structure that could capture elements of non-stationarity [31]. Alternatively, the ability to use state-of-the-art MCMC and estimate a reliable posterior expectation might create resilience to overfitting. The training/testing error for  $\pi$ VAE is 0.07/0.38, while the full rank GP is 0.002/2.47. Therefore the training error is 37 times smaller in the GP, but the testing error is only 6 times smaller in  $\pi$ VAE suggesting that, despite marginalisation, the GP is still overfitting.

Method	RMSE	NLL
Full rank GP	0.099	-0.258
$\pi$ VAE	0.112	0.006
SGPR ( $m = 512$ )	0.273	0.087
SVGP ( $m = 1024$ )	0.268	0.236

Table 1: Test results for  $\pi$ VAE, a full rank GP and approximate algorithms SGPR and SVGP on *Kin40K*.

Table 1 compares  $\pi$ VAE on the *Kin40K* [34] dataset to state-of-the-art full and approximate GPs, with results taken from Wang et al. [35]. The objective was to predict the distance of a robotic arm from the target given the position of all 8 links present on the robotic arm. In total we have 40,000 samples which are divided randomly into  $\frac{2}{3}$  training samples and  $\frac{1}{3}$  test samples. We train  $\pi$ VAE on  $10^7$  functions drawn from an 8-D GP, observed at 200 locations, where each of the 8 dimensions had values drawn uniformly from the range  $(-2, 2)$  and lengthscale varied between  $10^{-3}$  to 10. Once  $\pi$ VAE was trained on the prior function we use it to infer the posterior distribution for the training examples in *Kin40K*. Table 1 shows results for RMSE and negative log-likelihood (NLL) of  $\pi$ VAE against various GP methods on test samples. The full rank GP results reported in Wang et al. [35] are better than those we obtain from  $\pi$ VAE, but we are competitive, and far better than the approximate GP methods. We also note here that the exact GP is based on maximum marginal likelihood while  $\pi$ VAE performs full Bayesian inference; all posterior checks were excellent showing calibration both in uncertainty and point estimates. For detailed diagnostics see the Appendix.

Finally, we apply  $\pi$ VAE to the task of reconstructing MNIST digits from partial observations. We first train our  $\pi$ VAE on MNIST digits train dataset (not partial) with 40 latent dimensions. Encoder has 256 and 128 hidden units in first and second layer respectively. Images in testing are sampled such that only 10, 20 or 30% of pixel values are used and then  $\pi$ VAE predicts the intensity at all other pixel locations. As seen from Fig. 7(Appendix), the performance of  $\pi$ VAE increases with pixel density, but even with 10% of pixels our model is able to learn a decent approximation of the image. The uncertainty in prediction can be seen from the different samples produced by the model for the same data. As the number of given locations increases, the variance between samples decreases with quality of the image also increasing.

## 4 Discussion and Conclusion

In this paper we have proposed a novel VAE formulation of a stochastic process, with the ability to learn function classes and properties of functions. Our  $\pi$ VAEs typically have a small (5-50), uncorrelated latent dimension of parameters, so Bayesian inference with MCMC is straightforward and highly effective at successfully exploring the posterior distribution. This accurate estimation of uncertainty is essential in many areas such as medical decision-making.

$\pi$ VAE combines the power of deep learning to create high capacity function classes, while ensuring tractable inference using fully Bayesian MCMC approaches. Our 1-D example in Figure 2 demonstrates that an exciting use of  $\pi$ VAE is to incorporate domain knowledge about the problem. Monotonicity or complicated dynamics can be encoded directly into the prior [36] on which  $\pi$ VAE is trained. Our log-Gaussian Cox Process example shows that not only functions can be modelled, but also properties of functions such as integrals. Perhaps the most surprising result is the performance of the  $\pi$ VAE on spatial interpolation. Despite being trained on samples from a Gaussian process,  $\pi$ VAE substantially outperforms a full rank GP. We conjecture this is due to the more complex structure of the feature representation  $\Phi$  and due to a resilience to overfitting. The MNIST example highlights how  $\pi$ VAE can be used as a generative model on a much smaller subset of training data.

There are costs to using  $\pi$ VAE, especially the large upfront cost in training. For complex priors, training could take days or weeks and will invariably require the heuristics and parameter searches inherent in applied deep learning to achieve a good performance. However, once trained, a  $\pi$ VAE network is applicable on a wide range of problems, with the Bayesian inference MCMC step taking seconds or minutes.

Future work should investigate the performance of  $\pi$ VAE on higher dimensional settings (input spaces  $> 10$ ). Other stochastic processes, such as Dirichlet processes, should also be considered.

## 5 Broader Impact

Our work provides a scalable method to fit highly complex models using state-of-the-art MCMC approaches. We hope this method will be adopted by those looking to include domain knowledge in modelling complex phenomenon. However, given little is still known about disentanglement in VAEs, researches should be careful in over interpreting results from  $\pi$ VAE as causal or representative of a fully constrained mechanism. In addition, as VAE's improve, our method will be susceptible to individuals creating fake data in bad faith.

## References

- [1] Sheldon M Ross. *Stochastic processes*, volume 2. John Wiley & Sons, 1996.
- [2] Carl Edward Rasmussen and Christopher K. I. Williams. *Gaussian processes for machine learning*. Adaptive computation and machine learning. MIT Press, 2006. ISBN 026218253X. URL <http://www.worldcat.org/oclc/61285753>.
- [3] Charles E Antoniak. Mixtures of dirichlet processes with applications to bayesian nonparametric problems. *The annals of statistics*, pages 1152–1174, 1974.
- [4] Jesper Møller, Anne Randi Syversveen, and Rasmus Plenge Waagepetersen. Log gaussian cox processes. *Scandinavian Journal of Statistics*, 25(3):451–482, 1998. doi: 10.1111/1467-9469.00115.
- [5] Alan G. Hawkes. Spectra of some self-exciting and mutually exciting point processes. *Biometrika*, 58(1):83–90, 1971. ISSN 00063444. doi: 10.1093/biomet/58.1.83.
- [6] Daniel M. Roy and Yee Whye Teh. The Mondrian process. In *Advances in Neural Information Processing Systems 21 - Proceedings of the 2008 Conference*, 2009. ISBN 9781605609492.
- [7] Finn Lindgren, Håvard Rue, and Johan Lindström. An explicit link between Gaussian fields and Gaussian Markov random fields: the stochastic partial differential equation approach. *Journal of the Royal Statistical Society: Series B (Statistical Methodology)*, 73(4):423–498, 2011. ISSN 13697412. doi: 10.1111/j.1467-9868.2011.00777.x.
- [8] Arthur Jacot, Franck Gabriel, and Clément Hongler. Neural tangent kernel: Convergence and generalization in neural networks. In *Advances in Neural Information Processing Systems*, 2018.
- [9] R. Neal. Bayesian Learning for Neural Networks. *LECTURE NOTES IN STATISTICS -NEW YORK- SPRINGER VERLAG-*, 1996. ISSN 0930-0325.
- [10] Michael Betancourt, Simon Byrne, Sam Livingstone, and Mark Girolami. The geometric foundations of Hamiltonian Monte Carlo. *Bernoulli*, 2017. ISSN 13507265. doi: 10.3150/16-BEJ810.
- [11] Thomas P. Minka. Expectation propagation for approximate bayesian inference. In *Proceedings of the Seventeenth Conference on Uncertainty in Artificial Intelligence*, UAI’01, page 362–369, San Francisco, CA, USA, 2001. Morgan Kaufmann Publishers Inc. ISBN 1558608001.
- [12] Hippolyt Ritter, Aleksandar Botev, and David Barber. A scalable laplace approximation for neural networks. In *6th International Conference on Learning Representations, ICLR 2018 - Conference Track Proceedings*, 2018.
- [13] Balaji Lakshminarayanan, Alexander Pritzel, and Charles Blundell. Simple and scalable predictive uncertainty estimation using deep ensembles. In *Advances in Neural Information Processing Systems*, 2017.
- [14] Max Welling and Yee Whye Teh. Bayesian learning via stochastic gradient langevin dynamics. In *Proceedings of the 28th International Conference on Machine Learning, ICML 2011*, 2011. ISBN 9781450306195.

- [15] Charles Blundell, Julien Cornebise, Koray Kavukcuoglu, and Daan Wierstra. Weight uncertainty in neural networks. In *32nd International Conference on Machine Learning, ICML 2015*, 2015. ISBN 9781510810587.
- [16] Yuling Yao, Aki Vehtari, Daniel Simpson, and Andrew Gelman. Yes, but did it work?: Evaluating variational inference. In *35th International Conference on Machine Learning, ICML 2018*, 2018. ISBN 9781510867963.
- [17] Jonathan H Huggins, Mikołaj Kasprzak, Trevor Campbell, and Tamara Broderick. Practical posterior error bounds from variational objectives. *arXiv preprint arXiv:1910.04102*, 2019.
- [18] Matthew D Hoffman, David M Blei, Chong Wang, and John Paisley. Stochastic variational inference. *The Journal of Machine Learning Research*, 14(1):1303–1347, 2013.
- [19] Jiayu Yao, Weiwei Pan, Soumya Ghosh, and Finale Doshi-Velez. Quality of uncertainty quantification for bayesian neural network inference. *arXiv preprint arXiv:1906.09686*, 2019.
- [20] Diederik P. Kingma and Max Welling. Auto-Encoding Variational Bayes (VAE, reparameterization trick). *ICLR 2014*, 2014.
- [21] Danilo Jimenez Rezende, Shakir Mohamed, and Daan Wierstra. Stochastic backpropagation and approximate inference in deep generative models. In *International Conference on Machine Learning*, pages 1278–1286, 2014.
- [22] Bob Carpenter, Andrew Gelman, Matthew D. Hoffman, Daniel Lee, Ben Goodrich, Michael Betancourt, Marcus Brubaker, Jiqiang Guo, Peter Li, and Allen Riddell. Stan : A Probabilistic Programming Language. *Journal of Statistical Software*, 76(1):1–32, 2017. ISSN 1548-7660. doi: 10.18637/jss.v076.i01.
- [23] Geoffrey E Hinton and Ruslan R Salakhutdinov. Reducing the dimensionality of data with neural networks. *science*, 313(5786):504–507, 2006.
- [24] Diederik P Kingma and Max Welling. An introduction to variational autoencoders. *Foundations and Trends® in Machine Learning*, 12(4):307–392, 2019.
- [25] Marta Gamelo, Dan Rosenbaum, Chris J. Maddison, Tiago Ramalho, David Saxton, Murray Shanahan, Yee Whye Teh, Danilo J. Rezende, and S. M. Ali Eslami. Conditional neural processes. In *35th International Conference on Machine Learning, ICML 2018*, 2018. ISBN 9781510867963.
- [26] Hyunjik Kim, Andriy Mnih, Jonathan Schwarz, Marta Gamelo, S M Ali Eslami, Dan Rosenbaum, Oriol Vinyals, and Yee Whye Teh. Attentive Neural Processes. *CoRR*, abs/1901.0, 2019.
- [27] Ali Rahimi and Benjamin Recht. Random features for large-scale kernel machines. In *Advances in neural information processing systems*, pages 1177–1184, 2008.
- [28] Anonymous.  $\pi$ VAE: Encoding stochastic process priors with variational autoencoders (Appendix). In *Proceedings of the 37th International Conference on Machine Learning, ICML 2020*, 2020.
- [29] José Miguel Hernández-Lobato and Ryan Adams. Probabilistic backpropagation for scalable learning of bayesian neural networks. In *International Conference on Machine Learning*, pages 1861–1869, 2015.
- [30] Radford M Neal. *Probabilistic inference using Markov chain Monte Carlo methods*. Department of Computer Science, University of Toronto Toronto, Ontario, Canada, 1993.
- [31] J.-F. Ton, S. Flaxman, D. Sejdinovic, and S. Bhatt. Spatial mapping with Gaussian processes and nonstationary Fourier features. *Spatial Statistics*, 2018. ISSN 22116753. doi: 10.1016/j.spasta.2018.02.002.
- [32] Jacob R. Gardner, Geoff Pleiss, David Bindel, Kilian Q. Weinberger, and Andrew Gordon Wilson. Gpytorch: Blackbox matrix-matrix Gaussian process inference with GPU acceleration. In *Advances in Neural Information Processing Systems*, 2018.

- [33] Håvard Rue, Sara Martino, and Nicolas Chopin. Approximate Bayesian inference for latent Gaussian models by using integrated nested Laplace approximations. *Journal of the Royal Statistical Society. Series B: Statistical Methodology*, 71(2):319–392, 4 2009. ISSN 13697412. doi: 10.1111/j.1467-9868.2008.00700.x.
- [34] Anton Schwaighofer and Volker Tresp. Transductive and inductive methods for approximate gaussian process regression. In *Advances in Neural Information Processing Systems*, pages 977–984, 2003.
- [35] Ke Wang, Geoff Pleiss, Jacob Gardner, Stephen Tyree, Kilian Q Weinberger, and Andrew Gordon Wilson. Exact gaussian processes on a million data points. In *Advances in Neural Information Processing Systems*, pages 14622–14632, 2019.
- [36] Anthony L. Caterini, Arnaud Doucet, and Dino Sejdinovic. Hamiltonian variational auto-encoder. In *Advances in Neural Information Processing Systems*, 2018.
- [37] Adam Paszke, Sam Gross, Francisco Massa, Adam Lerer, James Bradbury, Gregory Chanan, Trevor Killeen, Zeming Lin, Natalia Gimelshein, Luca Antiga, et al. Pytorch: An imperative style, high-performance deep learning library. In *Advances in Neural Information Processing Systems*, pages 8024–8035, 2019.

Accompanying the submission  $\pi$ VAE: *Encoding stochastic process priors with variational autoencoders*.

## A MCMC diagnostics

Figure 5 presents the MCMC diagnostics for the 1-D GP function learning example shown in Figure 1. Both  $\hat{R}$  and effective sample size for all the inferred parameters (latent dimension of the VAE and noise in the observation) are well behaved with  $\hat{R} \leq 1.01$  (Figure 5(a)) and effective sample size greater than 1 (Figure 5(b)). Furthermore, even the draws from the posterior predictive distribution very well capture the true distribution in observations as shown in Figure 5(c).

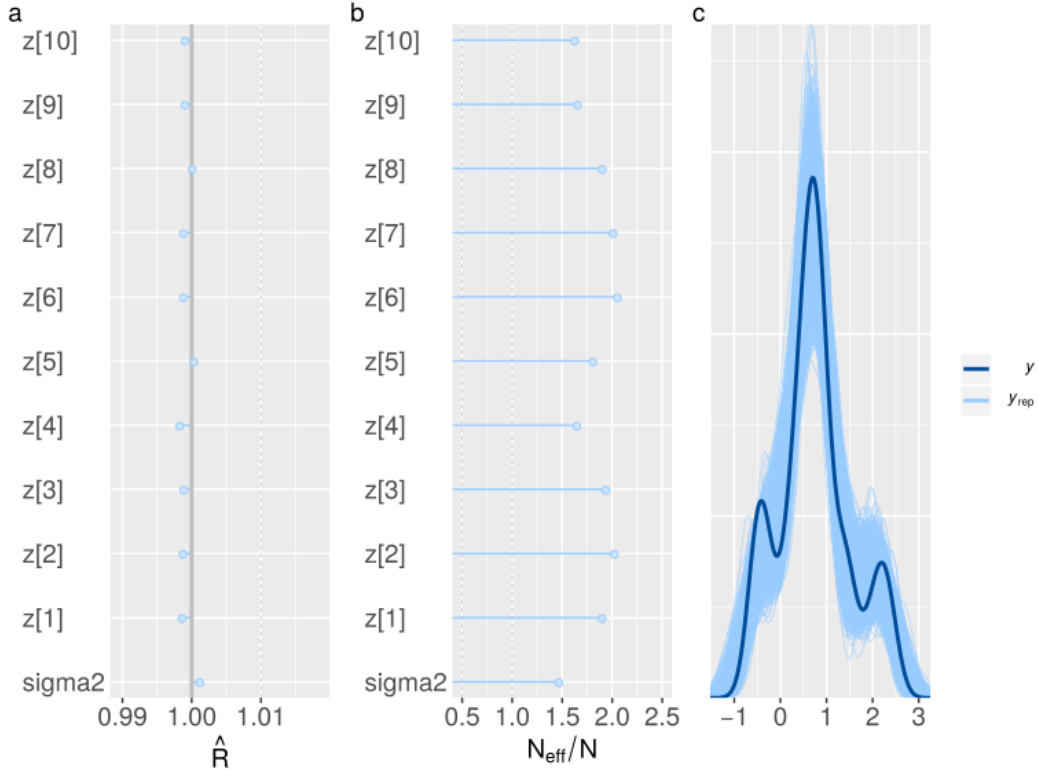


Figure 5: MCMC diagnostics for VAE inference presented in Figure 1: (a) and (b) shows the values for  $\hat{R}$  and  $\frac{N_{\text{eff}}}{N}$  for all parameters inferred with Stan. (c) shows the true distribution of observations along with the draws from the posterior predictive distribution.

Figure 6 presents the MCMC diagnostics for the kin40K dataset with  $\pi$ VAE as shown in Table 1. Both  $\hat{R}$  and effective sample size for all the inferred parameters (latent dimension of the VAE and noise in the observation) are well behaved with  $\hat{R} \leq 1.01$  (Figure 6(a)) and effective sample size greater than 0.5 (Figure 6(b)). Furthermore, the draws from the posterior predictive distribution are shown against the true distribution in observations as shown in Figure 6(c).

## B Algorithm

In the following section we provide the algorithm to train, simulate and infer parameters from  $\pi$ VAE.

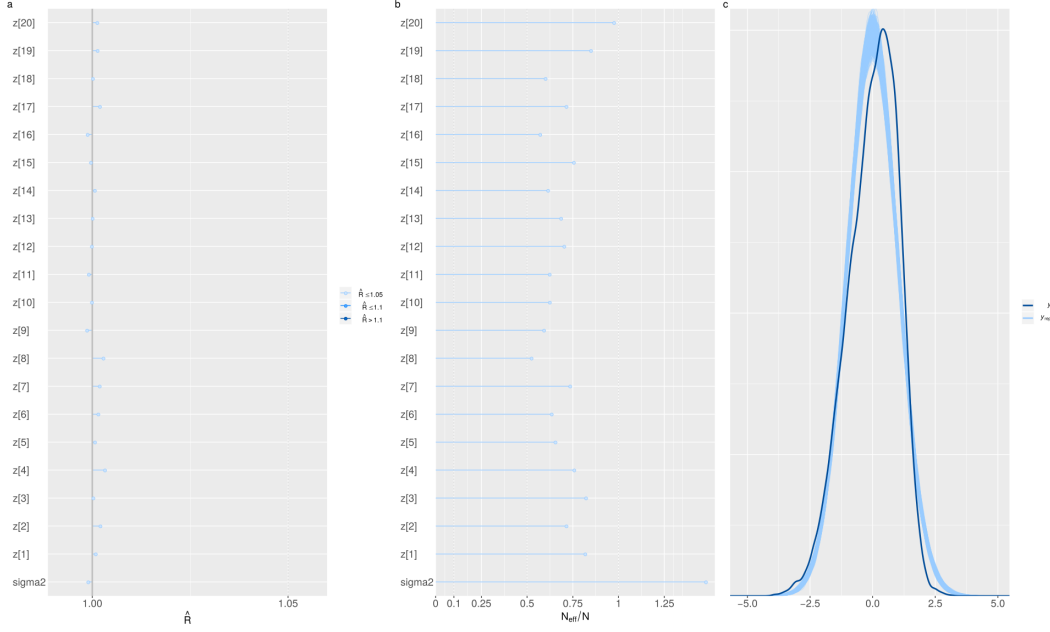


Figure 6: MCMC diagnostics for  $\pi$ VAE inference presented in Table 1: (a) and (b) shows the values for  $\hat{R}$  and  $\frac{N_{eff}}{N}$  for all parameters inferred with Stan. (c) shows the true distribution of observations along with the draws from the posterior predictive distribution.

---

**Algorithm 1** Prior Training for  $\pi$ VAE (stage 1)

---

- 1: Draw  $N$  functions evaluated at  $K$  points.  $s_i^k$  is an observed location with a given function value  $x_i^k$  such that  $i \in N$  and  $k \in K$
  - 2: **repeat**
  - 3:   **for** each function  $i$  **do**
  - 4:     **for** each location  $k$  **do**
  - 5:       transform locations:  $\Phi(s_i^k)$
  - 6:       multiply by linear basis:  $\hat{x}_{e,i}^k \leftarrow \beta_i^T \Phi(s_i^k)$
  - 7:     **end for**
  - 8:     append  $loss1$ :  $loss1 \leftarrow MSE(\hat{x}_{e,i}, x_i)$
  - 9:     encode  $\beta_i$  with VAE:  $[z_\mu, z_{sd}]^\top = e(\eta_e, \beta_i)$
  - 10:     reparameterize for  $\mathcal{Z}$ :  $\mathcal{Z} \sim \mathcal{N}(z_\mu, z_{sd}^2 \mathbb{I})$
  - 11:     decode with VAE,  $\hat{\beta}_i$ :  $\hat{\beta}_i = d(\eta_d, \mathcal{Z})$
  - 12:     **for** each location  $k$  **do**
  - 13:       transform locations:  $\Phi(s_i^k)$
  - 14:       multiply by decoded  $\hat{\beta}_i$ :  $\hat{x}_{d,i}^k = \hat{\beta}_i^\top \Phi(s_i^k)$
  - 15:     **end for**
  - 16:     append  $loss2$ :  $loss2 \leftarrow MSE(\hat{x}_{d,i}, x_i)$
  - 17:     minimize  $loss1 + loss2 + KL(\mathcal{Z} || \mathcal{N}(0, \mathbb{I}))$  to get  $\Phi, \beta_i, \eta_e, \eta_d$
  - 18:   **end for**
  - 19: **until** termination criterion satisfied (epochs)
- 

---

**Algorithm 2** Sampling and Inference from  $\pi$ VAE (stage 2)

---

- Require:** Trained decoder  $d$  ( $\eta_d$  fixed) and  $\Phi$
- 1: **Sampling:** Get  $J$  different locations where we need a sample function to be evaluated,  $s^j$  where  $j \in J$ .
  - 2: Sample  $\mathcal{Z}$ :  $\mathcal{Z} \sim \mathcal{N}(0, \mathbb{I})$
  - 3: decode with VAE to get,  $\beta$ :  $\beta = d(\eta_d, \mathcal{Z})$
  - 4: **for** each location  $j$  **do**
  - 5:   transform locations:  $\Phi(s^j)$
  - 6:   multiply by decoded  $\beta$ :  $\tilde{y}^j \leftarrow \beta^T \Phi(s^j)$
  - 7: **end for**
  - 8: **Inference:** Observed data has  $J$  different locations,  $s^j$  where  $j \in J$ , with corresponding function values,  $y^j$  where  $j \in J$ .
  - 9: Sample  $\mathcal{Z}$ :  $\mathcal{Z} \sim \mathcal{N}(z_\mu, z_{sd}^2 \mathbb{I})$
  - 10: decode with VAE to get,  $\beta$ :  $\beta = d(\eta_d, \mathcal{Z})$
  - 11: **for** each location  $j$  **do**
  - 12:   transform locations:  $\Phi(s^j)$
  - 13:   multiply by decoded  $\beta$ :  $\tilde{y}^j \leftarrow \beta^T \Phi(s^j)$
  - 14: **end for**
  - 15: Bayesian inference: for  $z_\mu, z_{sd}$  use unnormalised posterior distribution  $p(y_j | d, s_j, z_\mu, z_{sd}, \Phi) \mathcal{N}(z_\mu, z_{sd}^2 \mathbb{I})$   
Optimization (alternatively): minimize expected loss between  $\tilde{y}^j$  and  $y^j$ .
-

## C MNIST Example

Figure 7 below is the MNIST example referenced in the main test

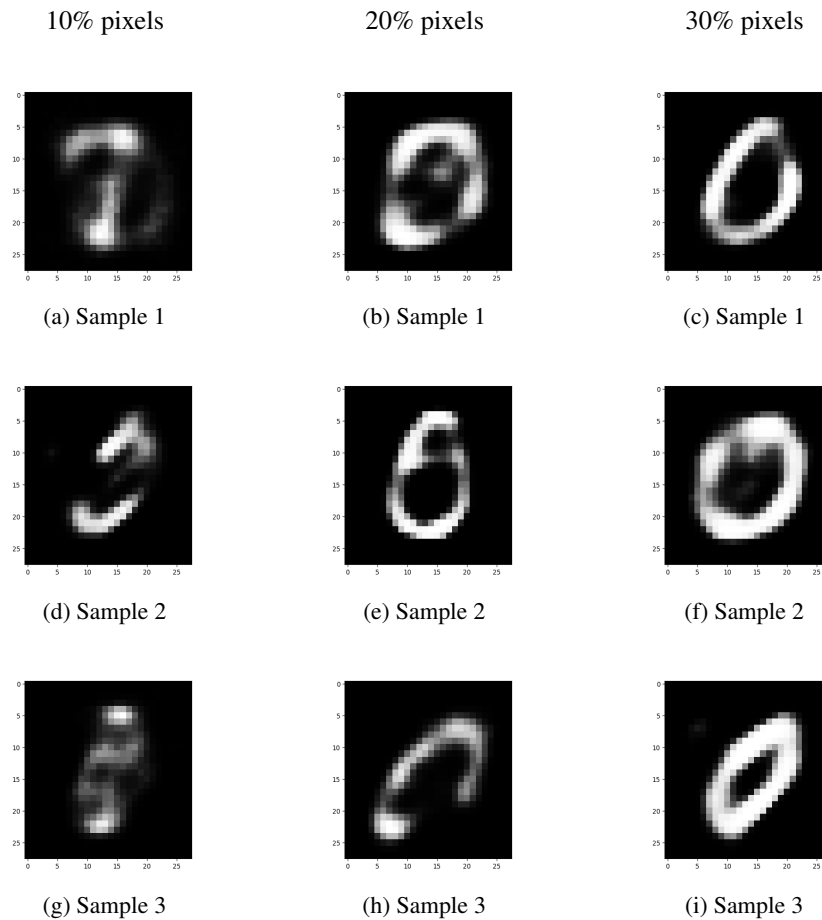


Figure 7: MNIST reconstruction after observing only 10, 20 or 30% of pixels from original data.

## D Implementation Details

All the models have been implemented with Pytorch [37] in Python. For Bayesian inference Stan [22] was used. For training while using a fixed grid, when not mentioned in main next, in each dimension we have used a range on -1 to 1. Our experiments ran on a workstation with two NVIDIA GeForce RTX 2080 Ti cards.